

MULTI-SENSOR OCEAN COLOUR ATMOSPHERIC CORRECTION FOR TIME-SERIES DATA: APPLICATION TO LANDSAT ETM+ AND OLI DATA

Samantha Lavender^{1,2}

1. Pixalytics Ltd, 1 Davy Road, Plymouth Science Park, Derriford, Plymouth, Devon, PL6 8BX, UK; [slavender\(at\)pixalytics.com](mailto:slavender(at)pixalytics.com)
2. School of Marine Science & Engineering, Plymouth University, Drake Circus, Plymouth, Devon, PL6 8AA, UK

ABSTRACT

This paper includes developments to a multi-sensor Atmospheric Correction (AC) that can be applied to marine and terrestrially-orientated medium resolution optical sensors, with a focus on the processing of imagery for coastal applications. The AC was originally developed for the airborne Compact Airborne Spectrographic Imager (CASI), and has since been expanded to include Compact High Resolution Imaging Spectrometer on the Project for On-Board Autonomy satellite mission (CHRIS-PROBA) with this paper detailing the extension to Landsat; examples shown are for the Landsat 7 Enhanced Thematic Mapper Plus (ETM+) and Landsat 8 Operational Land Imager (OLI).

The underlying approach is a Coastal Zone Color Scanner (CZCS) style aerosol estimation, using an Angstrom exponent, where the water's contribution to the Top Of Atmosphere (TOA) signal within the aerosol estimation wavebands is subtracted using a Bright Pixel (BP) estimation. This BPAC was originally developed for MEdium Resolution Imaging Spectrometer (MERIS), and includes a near infrared (NIR) optical water model. For Landsat, there is also an additional approach that extends the AC over the land using shortwave infrared (SWIR) vegetation 'dark targets' i.e. akin to the Dark Pixel (DP) approach over water.

The preliminary results appear promising, but further research is needed. Although the suspended particulate matter (SPM) maps have realistic patterns, spectral plots comparing the Landsat results to MERIS and Moderate Resolution Imaging Spectroradiometer on the Aqua spacecraft (MODISA) atmospherically corrected data appear to show that the reflectance values are too high and the spectral shape indicates the BPAC is failing in some areas for the Landsat ETM+ data.

INTRODUCTION

This paper outlines preliminary work being undertaken using Landsat 7 ETM+ and Landsat 8 OLI data as part of a broader multi-sensor AC activity, termed CASIDAS; please see Figure 1 for a schematic of the full multi-sensor approach. The Landsat series of instruments were primarily designed for terrestrial monitoring, but the ocean colour instruments (such as MERIS, MODISA and the Sea-Viewing Wide Field-of-View Sensor, SeaWiFS) have a limited spatial resolution and so are not ideal for understanding near-shore coastal and estuarine environments. In turn, the limitation of Landsat data has been the radiometric resolution, with 8-bit quantization, and low Signal-to-Noise Ratio (SNR) over dark targets such as water bodies. However Landsat 8 was launched in 2012 and carries two imaging instruments, OLI and the Thermal Infrared Scanner (TIRS); OLI acquires data in 8 spectral bands with 12-bit radiometric resolution and a 30 m spatial resolution.

The underlying AC approach is simplistic in nature, but allows the physics to be understood and the errors / uncertainties traced through the modules; initially developed first for CASI (1), then CHRIS-PROBA (2) and with the BP component also applied to SeaWiFS (3). The AC algorithm inherently has rules embedded within it, e.g., an AC should not produce negative land / water reflectances, which aids the solution choice when multiple solutions are considered equally valid. The ultimate future aim is not to have a single solution, i.e. single water-leaving reflectance spec-

trum for each pixel, but rather an ensemble of possible spectral solutions for which the mean and standard deviation are the AC output.

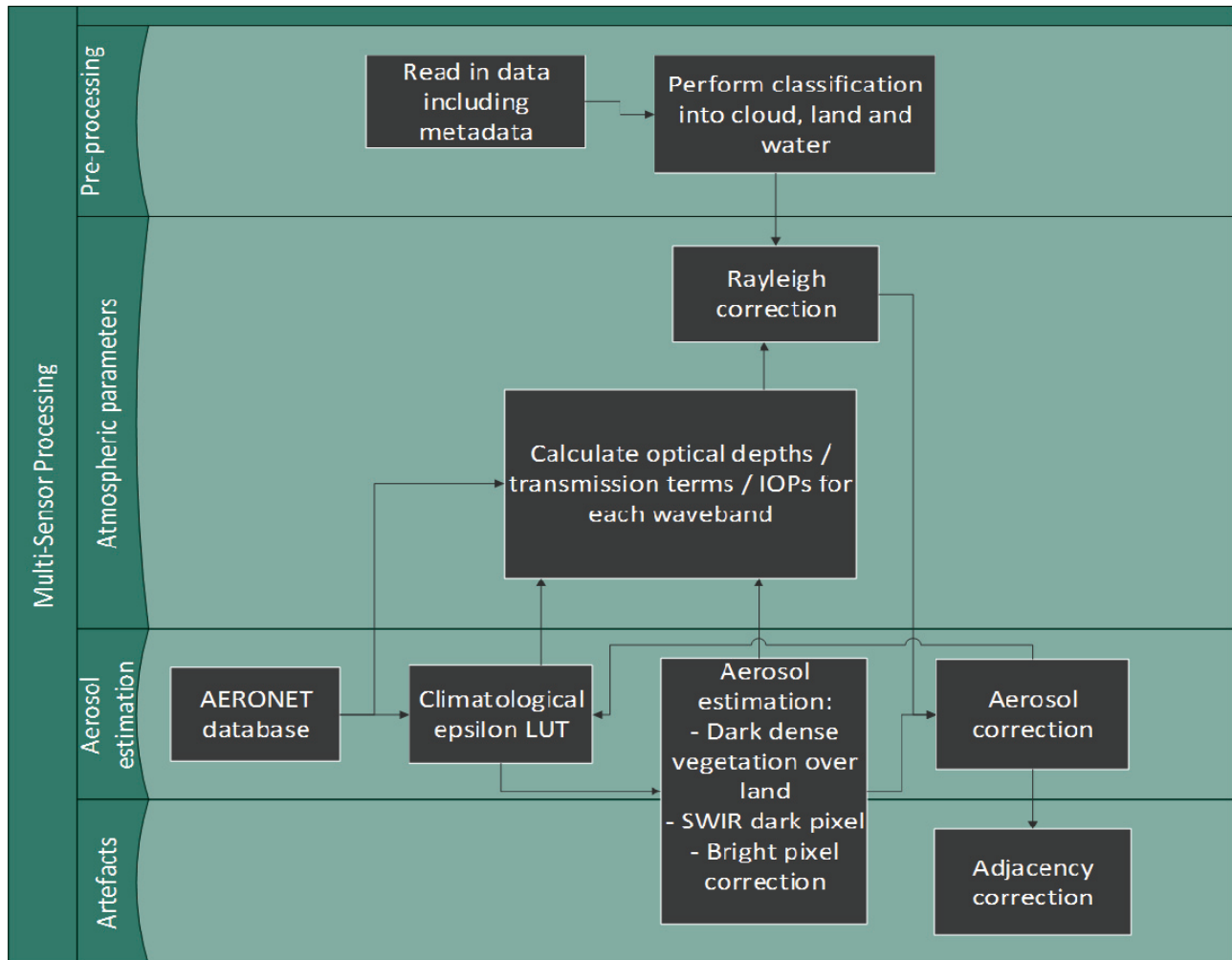


Figure 1: Schematic representing the overarching structure for the CASIDAS atmospheric correction approach.

Traditionally, the AC of ocean colour data has used the information available at the time of processing or updated meteorological data for offline processing. Typically the code also runs on a pixel-by-pixel basis with a lack of awareness about variability in space or time; there has been a limited use of spatial filtering e.g. since the 4th reprocessing in 2002 SeaWiFS waveband 7 (765 nm) radiance values are smoothed to minimize local variability in the NIR aerosol ratio (4) as significant pixelization / speckling effects were often found in the 1.1 km resolution data products (5). However, a change in focus from processing a pixel at a time to groups of pixels / time-series data allows the algorithm to receive and utilise information about the underlying spatial and temporal variability; with different scales of variability for the atmosphere and ocean. Within CASIDAS this is currently within the terrestrial AC that uses an area larger than the pixel to estimate the aerosol contribution and in future will also be through the use of Aerosol Robotic Network (AERONET) (6) data and a climatological Look-Up-Table (LUT) to remember the results of previous runs; a locational LUT is being built that contains the centre latitude / longitude and validity extent (spatially and temporally) for the monthly atmospheric AC parameters e.g. epsilon (ratio of the single scattering aerosol reflectance) climatology. This is so that the knowledge can be applied when data is reprocessed e.g. as a first guess for an iterative process, and / or to define boundaries within which atmospheric parameters can be constrained; especially when the sensor does not have the optimal wavebands.

THEORETICAL METHODOLOGY

The CASIDAS AC takes the total sensor detected reflectance $\rho_t(\lambda)$ and splits it into the total atmospheric path reflectance $\rho_{atm}(\lambda)$ and desired water-leaving reflectance $\rho_w(\lambda)$ that is reduced by the diffuse transmittance $t(\lambda)$ as it passed through the atmosphere:

$$\rho_t(\lambda) = \rho_{atm}(\lambda) + t(\lambda) \cdot \rho_w(\lambda) \quad (1)$$

The atmospheric path reflectance is itself split into the aerosol $\rho_a(\lambda)$ and Rayleigh $\rho_r(\lambda)$ path reflectance according to Eq. (2), with the Rayleigh scattering reflectance computed using a well-established theory (7). Without additional information the Rayleigh and atmospheric transmission corrections do not attempt to use actual meteorological values, but instead climatological values: atmospheric pressure of 1013.25 mbar; water vapour concentration of 2 g cm^{-2} ; ozone concentration of 0.33 atm cm:

$$\rho_{atm}(\lambda) = \rho_a(\lambda) + \rho_r(\lambda) \quad (2)$$

For Case I waters, the NIR water-leaving reflectance is assumed to be near zero (8) and so the DP AC approach is used. Eq. (1) can then be rewritten to give Eq. (3) when the Rayleigh reflectance is subtracted, leaving the Rayleigh corrected reflectance $\rho_{rc}(\lambda)$. The aerosol path reflectance, $\rho_a(\lambda)$ can then be calculated for NIR wavelengths (greater than 700 nm) using an exponential relationship to represent the assumed spectral behaviour of aerosol optical depth (9):

$$\rho_{rc}(\lambda > 700\text{nm}) = \rho_a(\lambda) \quad (3)$$

The aerosol extrapolation with wavelength is based on the CZCS model given by (4) that uses an Angstrom exponent, n :

$$\varepsilon(\lambda_i, \lambda_j) = \frac{\rho_a(\lambda_i)}{\rho_a(\lambda_j)} = \frac{\omega_a(\lambda_i) \cdot \tau_a(\lambda_i) \cdot p_a(\theta, \theta_0, \lambda_i)}{\omega_a(\lambda_j) \cdot \tau_a(\lambda_j) \cdot p_a(\theta, \theta_0, \lambda_j)} = \left(\frac{\lambda_i}{\lambda_j} \right)^{-n} \quad (4)$$

For Case I or II waters dominated by particulate scattering (termed BP), where the DP assumption no longer applies, the AC uses LUTs that hold standard values for the inherent optical properties (IOPs); absorption and backscattering of both the water and bio-optical constituents. Therefore, the NIR water reflectance at a given wavelength is a function of the optical properties of seawater, the optically active water constituents and the solar and viewing geometry. The optical effects of Coloured Dissolved Organic Matter (CDOM) and phytoplankton are assumed to be negligible in the NIR, which gives Eq. (5) that is solved for the two NIR wavebands using a non-linear, least squares, Newton-Raphson minimisation (10).

$$\rho_{rc}(\lambda) = \rho_t(\lambda) - \rho_r(\lambda) = \rho'_a + t(\lambda) \cdot f(\lambda, SPM, \theta_0, \theta, \phi) \quad (5)$$

Once estimated, the SPM NIR reflectance is subtracted from the Rayleigh corrected NIR reflectance values to give the NIR aerosol reflectance. The DP AC method is then applied to extrapolate this estimated NIR aerosol reflectance to the visible wavebands.

A new step in the process is that if the derived TOA Rayleigh and aerosol corrected reflectance is negative the Angstrom is iteratively adjusted positively/negatively from the starting value to see if a positive reflectance spectra can be achieved. At this stage of the algorithm development, the iteration stops when a positive reflectance spectra is achieved or the maximum iteration is reached and that value is used to produce the final BOA reflectance; in future it can be envisaged that several spectra are calculated, i.e., an ensemble result.

An AC is also applied over the land, with the aerosol reflectance estimated using SWIR vegetation ‘dark targets’ (11) with $\rho_t(SWIR) < 0.15$ following the approach of Masek (12) that is implemented for the Landsat Ecosystem Disturbance Adaptive Processing System (LEDAPS) (13). This is following the same reasoning as the above-water DP AC, i.e., by assuming that certain targets have negligible SWIR reflectance, the Rayleigh corrected SWIR reflectance is equivalent to the aerosol reflectance, i.e. Eq. (3). Targets that fulfil this criteria include green forests (11) alongside water itself.

PRACTICAL IMPLEMENTATION

The Landsat implementation has been tested on imagery from March 2003 and February 2014 geographically located over the southern North Sea (Landsat scenes referenced with the second World-wide Reference System, WRS-2, path 201 and row 023) where there is contemporaneous ocean colour data: MERIS Full Resolution (FR) image and Landsat ETM+ for the 24 March 2003; MODISA and Landsat OLI for the 26 February 2014.

For MERIS the two BPAC NIR wavebands are 12 (775 nm) and 13 (865 nm), while for MODIS the equivalent wavebands would be 15 (750 nm) and 16 (865 nm). For Landsat ETM+ the BPAC wavebands are 4 (830 nm) and 5 (1,670 nm), while the SWIR waveband is 7 (2,220 nm). For Landsat OLI these become wavebands 5 (865 nm), 6 (1,610 nm) and 7 (2,200 nm).

Figure 2 shows the stretched TOA reflectance for Landsat ETM+ wavebands 4 and 5. It is possible to see a signal from the water due to SPM close to the coast at 830 nm, but not at 1,670 nm; the SPM particles scatter the signal back out of the water, but the strong absorption by water itself increases exponentially as the wavelength increases from the red to NIR and then towards SWIR reducing the chance that scattering can occur. Therefore, the BPAC needs to correctly model (and subtract) the IOPs and hence reflectance signal originating from the water in waveband 4; the same is also true for the equivalent OLCI waveband.

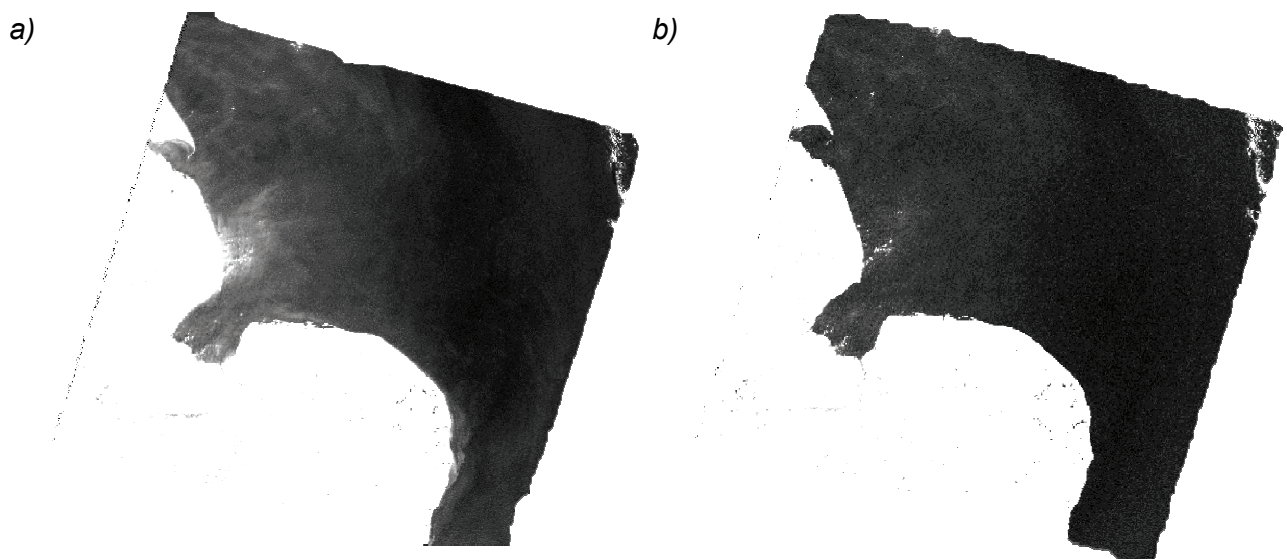


Figure 2: Landsat ETM+ 24 March 2003 TOA reflectance for wavebands (a) 4 and (b) 5; stretched to show the features in the water and so saturated over the land.

The MERIS data has been processed using ODESA version 1.2.4, including the MERIS Ground Segment development platform (MEGS) release 8.1 that contains an updated version of the BPAC (9), and the MODISA data was processed using SeaDAS version 7.0.1 that was run with the iterative NIR correction of Bailey et al. (14).

The preliminary processing of Landsat ETM+ and OLI has used climatological atmospheric values, but for contemporaneous MERIS processing we have in future the option of using the European Centre for Medium-Range Weather Forecasts fields stored within the Level 1 file and for SeaDAS processed data there is the National Centers for Environmental Prediction atmospheric pressure and water vapour data alongside the Total Ozone Mapping Spectrometer data retrievable from the web (<http://oceandata.sci.gsfc.nasa.gov/Ancillary/Meteorological/>).

RESULTS

Figure 3 shows the (a) MERIS TOA and (b) Landsat ETM+ TOA reflectance images from the 24 March 2003; both images show complex structures within the coastal waters resulting primarily from sediment erosion and resuspension. The (c) atmospherically corrected BOA reflectance

Landsat image and (d) SPM map, which is a by-product of the BPAC, are also shown and have the same marine features.

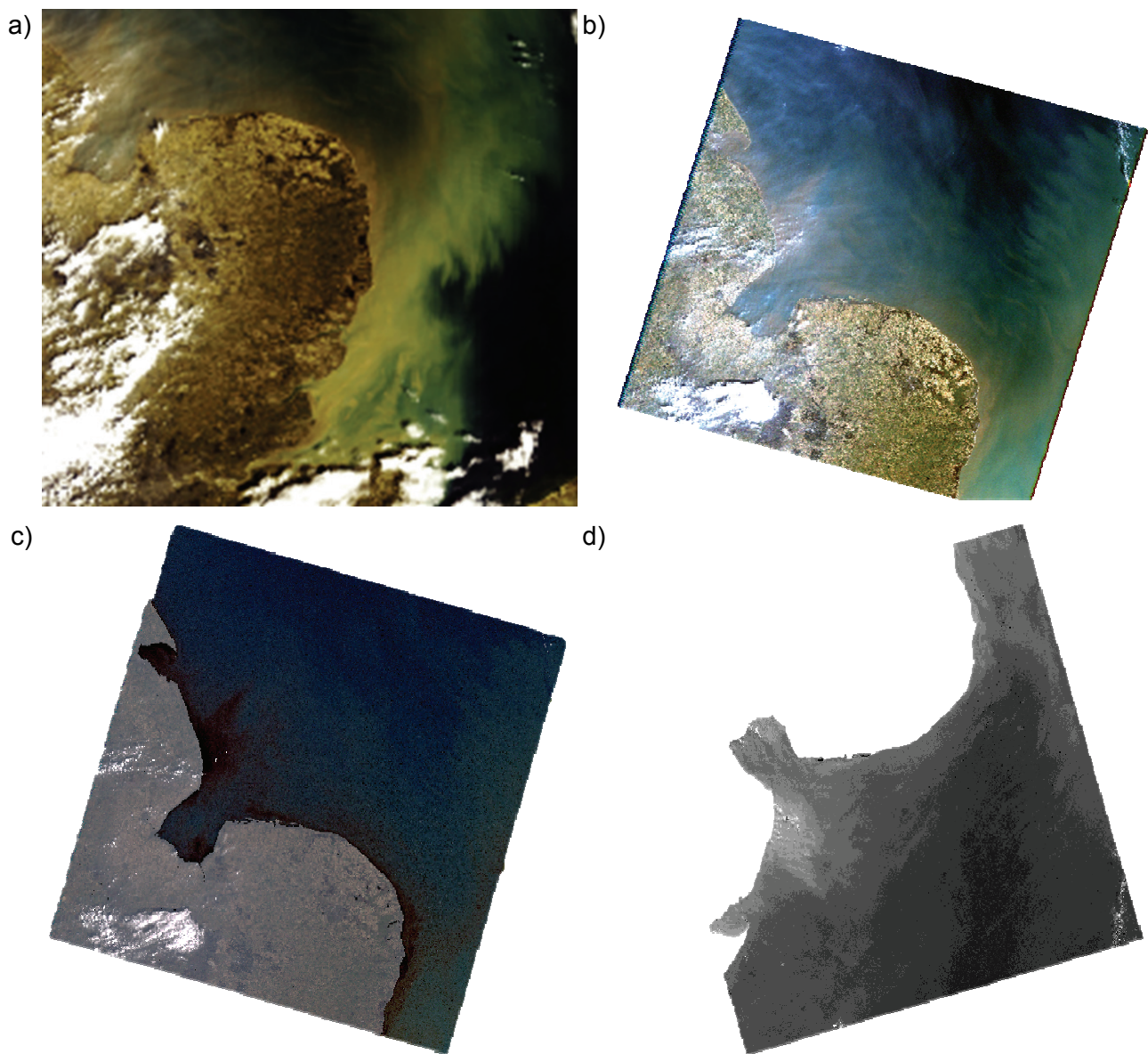


Figure 3: MERIS TOA image (a) from the 24 March 2003 with the Landsat ETM+ TOA reflectance image (b) on the same date, which is then atmospherically corrected to a BOA reflectance (c) and the (d) SPM image that's a bi-product of the AC process. For MERIS wavebands 7, 4 and 2 are being displayed a red, green and blue in the pseudo-true colour composites while for Landsat ETM+ it is wavebands 3, 2 and 1.

Over the land, the BOA image appears less blurred with some of the cloudy / cirrus cloud affected pixels appearing cloud free; no classification / cloud mask was applied and so the AC has been attempted in all cases (pixels) and works sometimes when there is cloud as this is treated as pixels having a high aerosol load. Over the water, the AC has partially failed around the coast where the pixels are red in colour (c) due to very low values for the blue/green water-leaving reflectances. The over-correction is because the BPAC is not correctly working; not predicting a sufficiently high NIR water signal and/or has the wrong Angstrom for the extrapolation of the aerosol signal to the visible wavebands. However, the SPM map shows the BPAC is switched on and providing a realistic pattern for the SPM concentrations despite the much lower SNR in the NIR than that commonly

available for an ocean colour sensor; the low SNR can be seen by the noisy nature of the atmospherically corrected water pixels.

Figure 4 shows the (a) MODISA BOA reflectance image and (b) Landsat OLI TOA reflectance image from the 26 February 2014; the MODISA image is distorted as the study area is at the edge of the MODISA swath, and the white areas show that the AC has failed around the coast (the land is coloured grey). The (c) atmospherically corrected Landsat image and (d) SPM map show patterns within the water similar to the MODISA and Landsat TOA imagery. For this date there was no obvious cloud or haze contamination for the Landsat scene, and so the qualitative difference between the TOA and BOA image is not significant.

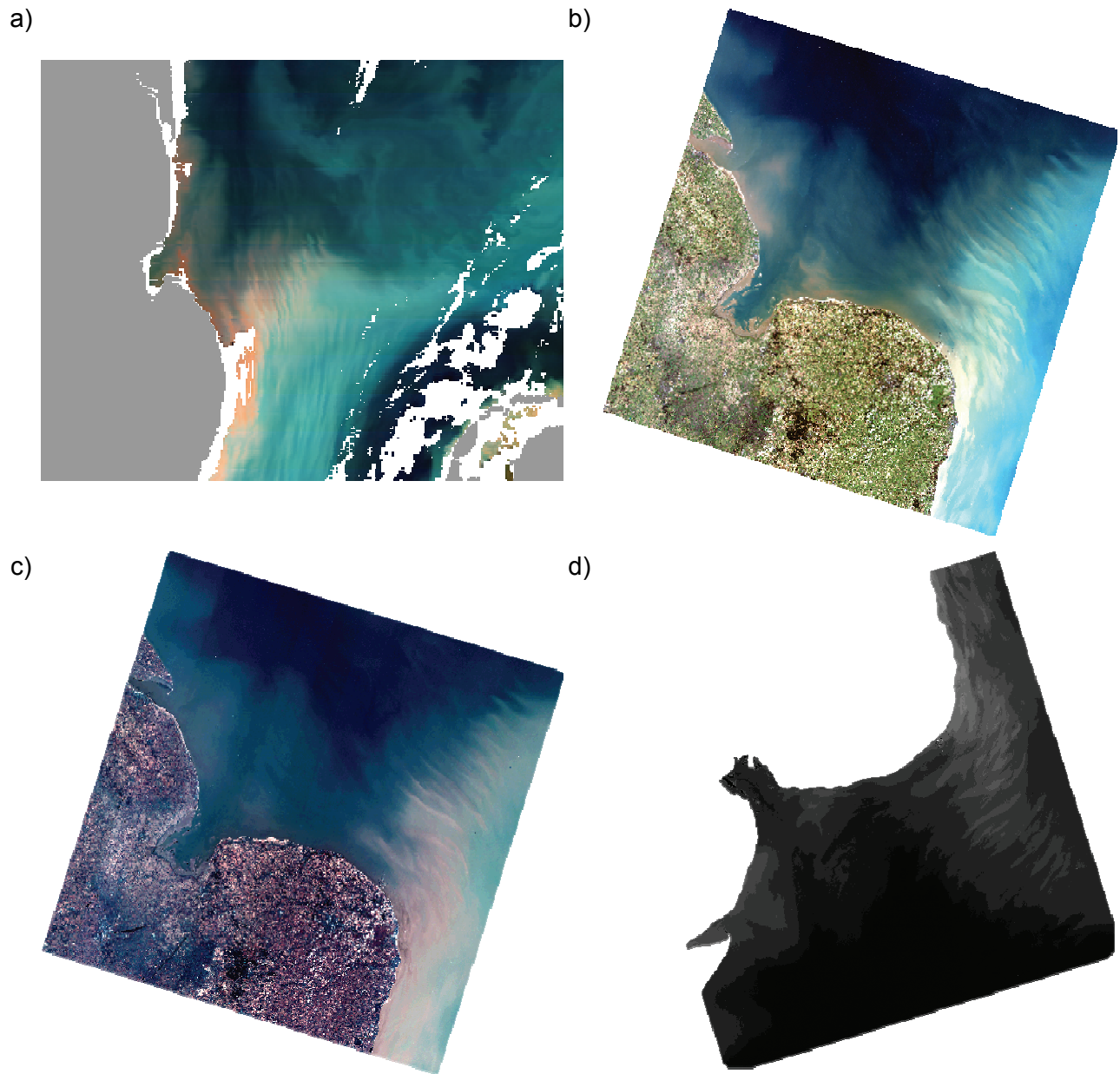


Figure 4: (a) MODISA BOA reflectance image from the 26 February 2014 with the corresponding (b) Landsat OLI TOA reflectance image on the same date, which is then atmospherically corrected to a (c) BOA reflectance and the (d) SPM image that's a bi-product of the AC process. For MODISA wavebands 9, 5 and 2 are being displayed a red, green and blue in the pseudo-true colour composites while for Landsat OLI it is wavebands 3, 2 and 1.

Unlike the ETM+ image, the OLI BPAC has not failed around coast and the improved SNR is noticeable as the atmospherically corrected imagery is not noisy; OLI is reported to have at least a

factor of eight improvement in the SNR compared to ETM+ (15) plus there is the improved radiometric quantization. There is also a waveband at 440 nm that is being displayed at the 'blue' band in the pseudo-true colour composites.

Figure 5 provides a preliminary comparison of the BOA spectral reflectance for three locations that correspond to decreasing turbidity, two near the coast and one further offshore; pixels in roughly the same geographical location were selected rather than exact matches as no account has been made for differences due to pixel size / sub-pixel variability and overpass times, and this area is highly dynamic. In all cases the Landsat spectra have higher values than the MERIS and MODISA spectra, which will be due to a number of factors e.g. no attempt to refine the Landsat calibration in addition to no correction for adjacency (due to the proximity to clouds or land), the bidirectional reflectance distribution function (BRDF) and surface / sun glitter or whitecaps.

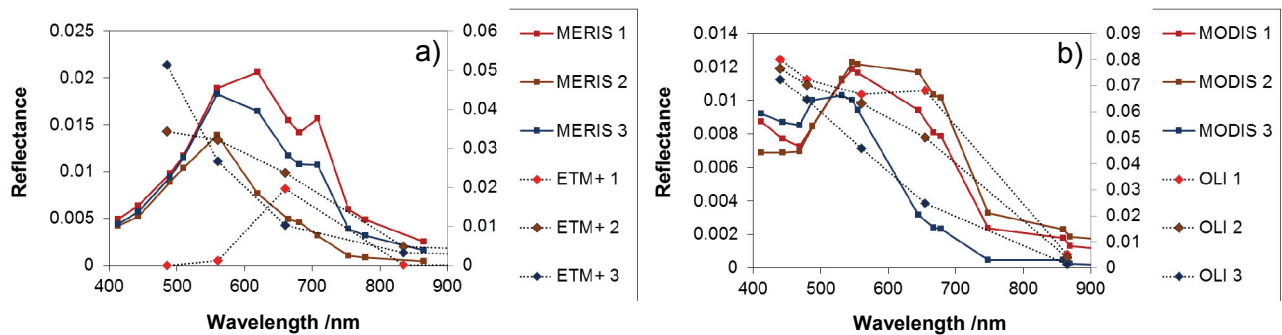


Figure 5: (a) MERIS and Landsat ETM+ extracted BOA spectra for March 2003 and (b) MODISA and Landsat OLI extracted BOA spectra for February 2014. The MERIS and MODISA data are on the primary y-axis, while the Landsat data is on the secondary y-axis as the values are significantly higher.

The spectral shape for the Landsat ETM+ data (Figure 5a) shows that in location 1 (red diamonds and black line for ETM+) the BP has failed to be applied correctly with near zero values for the blue and green wavebands. Location 3 (blue diamonds and black line for ETM+) appears to indicate that insufficient Rayleigh reflectance has been subtracted from the ETM+ data, which may be due to the use of a standard rather than actual atmospheric pressure and / or the geometry calculation that needs improving (16); the provided data has already been reprojected to a Universal Transverse Mercator (UTM) projection and the sensor-pixel-solar geometry is currently represented by a single set of angles calculated from values in the Metadata (MTL) file. The Landsat OLI data (Figure 5b) also appears to indicate that insufficient Rayleigh reflectance may have been subtracted as the spectral shapes also have values for the first 2 wavebands.

CONCLUSIONS

Several areas where the approach can be improved have already been identified. The geometry of each pixel needs to be calculated more accurately and the AC run with the available, rather than climatological, ancillary information. If not sufficiently subtracted, Rayleigh reflectance will influencing both the magnitude, making the values higher than expected, and spectral shape. The code will also be updated to include corrections for adjacency, the bidirectional reflectance distribution function (BRDF), surface / sun glitter and whitecaps. Franz et al. (16) also propose that the full-bandpass values are adjusted to that for square 11-nm band-passes and vicarious calibration gains are applied.

In addition, depending on the wind direction, the aerosol sources (continental, marine and anthropogenic) will vary with the relative humidity often controlling the aerosol size. LEDAPS (13) uses the AERONET (3) data to aid the Landsat aerosol property estimation, and this approach is envisaged in the future (AERONET box within Figure 1). However, there are limited coastal AERONET sites and they do not exist over the open ocean so this approach will also use previously derived ocean colour aerosol information to aid the Landsat processing.

The ultimate aim is that this approach represents a significant departure from current research where the target has often been to achieve the 'best result' on a pixel-basis as judged by the comparison to *in situ* point match-ups. All pixels are processed and the results are only disregarded when the AC fails; in the future a quality control flag will provide an indication of processing uncertainty.

With the upcoming missions planned within Europe, the dataset will also be expanded to include the Copernicus missions: the 'Landsat-like' Sentinel-2 Multi Spectral Instrument (MSI) and 'MERIS-like' Sentinel-3 Ocean and Land Colour Instrument (OLCI) plus potentially the optical wavebands from the Sea and Land Surface Temperature Radiometer (SLSTR).

ACKNOWLEDGEMENTS

Landsat 7 ETM+ and OLI data is courtesy of NASA/USGS and obtained using Glovis/EarthExplorer. MERIS data is courtesy of ESA with research supported through the ESA-AO 533 and ODESA courtesy of ESA and ACRI-ST. MODISA data and SeaDAS is courtesy of the NASA Ocean Biology Processing Group (OBPG). The atmospheric correction was originally developed through the NERC small grant (NER/M/S/2000/00293, PI Lavender) with CASI data from the NERC Airborne Research and Survey Facility.

REFERENCES

- 1 Lavender S J & C R C Nagur, 2002. Mapping UK coastal waters with high resolution imagery. *Journal of Optics A: Pure and Applied Optics*, 4: S50-S55
- 2 Lavender S J, C R C Nagur & D Doxaran, 2005. [High spatial resolution remote sensing of the Plymouth coastal waters](#), 4 pp. [Proceedings of the 3rd ESA CHRIS/Proba Workshop](#) (21-23 March, ESRIN, Frascati, Italy) ESA SP-593, June 2005
- 3 Lavender S J, M H Pinkerton, G F Moore, J Aiken & D Blondeau-Patissier, 2005. Modification to the atmospheric correction of SeaWiFS ocean colour images over turbid waters. [Continental Shelf Research](#), 25: 539-555
- 4 NASA, 2002. [Atmospheric correction](#) (last date accessed: 31 Mar 2014)
- 5 Hu C, K L Carder & F E Muller-Karger, 2000. Atmospheric correction of SeaWiFS imagery: assessment of the use of alternative bands. [Applied Optics](#), 39, 3573-3581
- 6 Holben, B N, T F Eck, I Slutsker, D Tanre, J-P Buis, A Setzer, E Vermote, J A Reagan, Y J Kaufman, T Nakajima, F Lavenu, I Jankowiak & A Smirnov, 1998. AERONET – A federated instrument network and data archive for aerosol characterization, [Remote Sensing of Environment](#), 66: 1-13
- 7 Cornette W M & J G Shanks, 1992. Physically reasonable analytic expression for the single-scattering phase function. [Applied Optics](#), 31: 3152-3160
- 8 Gordon H R & D K Clark, 1981. Clear water radiances for atmospheric correction of Coastal Zone Color Scanner imagery. [Applied Optics](#), 20: 4175-4180
- 9 Gordon H R & M Wang, 1994. Retrieval of water-leaving radiance and aerosol optical thickness over the oceans with SeaWiFS: a preliminary algorithm. [Applied Optics](#), 33: 443-452
- 10 Moore G F, J Aiken & S J Lavender, 1999. The atmospheric correction of water colour and the quantitative retrieval of suspended particulate matter in Case II Waters: application to MERIS. [MERIS Special Issue, International Journal of Remote Sensing](#), 20: 1713-1733
- 11 Kaufman Y J, A E Wald, L A Remer, B-C Gao, R-R Li & L Flynn, 1997. The MODIS 2.1- μ m channel - Correlation with visible reflectance for use in remote sensing of aerosol. [IEEE Transactions on Geoscience and Remote Sensing](#), 35(5): 1286-1298

- 12 Masek, J G, E F Vermote, N Saleous, R Wolfe, F G Hall, F Huemmrich, F Gao, J Kutler & T K Lim, 2006. A Landsat surface reflectance data set for North America, 1990-2000. Geoscience and Remote Sensing Letters, 3: 68-72
- 13 Masek, J G, E F Vermote, N Saleous, R Wolfe, F G Hall, F Huemmrich, F Gao, J Kutler, & T K Lim, 2012. LEDAPS Landsat calibration, reflectance, atmospheric correction reprocessing code. Model product. Oak Ridge National Laboratory Distributed Active Archive Center, Oak Ridge, Tennessee, U.S.A. <http://dx.doi.org/10.3334/ORNLDAAAC/1080>
- 14 Bailey S W, B A Franz & P J Werdell, 2010. Estimation of near-infrared water-leaving reflectance for satellite ocean color data processing. Optics Express, 18: 7521-7527
- 15 Irons J R, J L Dwyer & J A Barsi, 2012. The next Landsat satellite: The Landsat Data Continuity Mission. Remote Sensing of Environment, 122: 11-21
- 16 Franz, B A, S W Bailey, N Kuring & P J Werdell, 2014. Ocean Color Measurements from Landsat-8 OLI using SeaDAS, Proceedings Ocean Optics 2014 (Portland, Maine, U.S.A.) 26-31 October 2014